applied sciences

MDPI

Article

Hybrid Harmonic Suppression Method at DC Link of Series-Connected 18-Pulse Rectifier

Quanhui Li, Xinyu Yin, Fangang Meng *, Xiao He, Gaojie Wang and Changxing Guo

School of Electrical Engineering and Automation, Harbin Institute of Technology, Harbin 150001, China; liquanhui0413@163.com (Q.L.); yxy06281205@163.com (X.Y.); hx02190401@163.com (X.H.); wgj_hit@163.com (G.W.); 15954127800@163.com (C.G.)
* Correspondence: mfg0327@sina.com

Featured Application: The proposed rectifier is suitable for aviation power system and ship power system which require high overload capacity and reliability.

Abstract: To suppress the harmonics of series-connected 18-pulse rectifier, a hybrid harmonic suppression method is proposed in this paper. According to the structure of the converter and the KVL, the injection voltages are expressed. According to the injection voltages, the relation between the input voltage THD and the injection transformer turn ratio is obtained. Based on the relationship, when the THD of the input voltage researches the lowest value, the optimal injection transformer turn ratio is determined. Testing result shows that after using the proposed reduction method, the input side THD values of the converter are reduced. The capacity of the suppression circuit is only about 2% of the load power. The proposed converter is qualified for the interface between the AC generator and the DC bus of the aircraft electrical system.

Keywords: harmonic injection; hybrid harmonic suppression; injection transformer; series-connected multipulse rectifier

check for updates

Citation: Li, Q.; Yin, X.; Meng, F.; He, X.; Wang, G.; Guo, C. Hybrid Harmonic Suppression Method at DC Link of Series-Connected 18-Pulse Rectifier. *Appl. Sci.* **2022**, *12*, 5544. https://doi.org/10.3390/app12115544

Academic Editors: Hongchen Liu, Jiandong Duan and Fengjiang Wu

Received: 26 April 2022
Accepted: 16 May 2022
Published: 30 May 2022

1. Introduction

Because of their simple structure and strong robustness, multipulse rectifiers (MPRs) widely serve as interfaces between AC generators and DC buses in small, isolated power systems, such as aircraft electrical systems and ship power systems [1–3]. However, due to the nonlinearity of the diodes, a lot of harmonic pollution is produced [4–6].

Usually, there are two types of methods to suppress the harmonic pollution. The first method improves the harmonic suppression ability by increasing the output phases of the multi-winding, phase-shifting transformers [7–11]. In [7], a 15-output autotransformer is proposed; in [8], a T-connected transformer is installed to suppress harmonics; in [9], a Z/z transformer is proposed; in [10], the 3/9 and 3/12 isolation transformer are researched; in [11], a round-shaped transformer is proposed. Through analyzing the structure of the multi-winding transformer in [7–11], the first method can suppress the harmonics of input currents and ripples of load voltages simultaneously, and its harmonic suppression ability is associated with the output phases number of transformer. However, with the increase in the output phases, the asymmetry factors, and the production difficulty and cost of the multi-winding transformer increase rapidly. Therefore, increasing output phase number is not an economic method.

The harmonic reduction methods are divided into the passive methods, the active methods, and the hybrid methods. The passive methods, such as [12], generally use injection transformers and diodes to suppress harmonics, which have high reliability but limited reduction ability. The active methods generally use injection transformers and switches [13,14], and compared with the passive methods, the harmonic reduction ability is increased but the reliability is reduced. To solve the problems of the passive methods and the active methods, the hybrid methods are proposed. The hybrid methods, such as [15], use injection transformers, diodes, and switches to suppress harmonics. From [15], the hybrid methods are the combination of the passive methods and the active methods, the low-order harmonics are suppressed by the passive part, while the high-order harmonics are suppressed by the active part. Compared with the passive methods and the active methods, the harmonic suppression ability and the reliability are enhanced.

To increase the output voltage level and improve the input power quality of the converter, this paper combines multi-winding phase-shifting transformer based on [16], and the hybrid harmonic reduction method to suppress the harmonics of MPRs, which not only improves the output voltage level, but also improves the input power quality. The converter has high reliability, output voltage level, and input power quality, which qualify it for the interface between the AC generator and the DC bus of an aircraft electrical system.

2. The Proposed Rectifier with Harmonic Injection Circuit

2.1. Phase-Shifting Transformer Design

The proposed multipulse rectifier with multi-winding phase-shifting transformer and hybrid harmonic reduction method is shown in Figure 1. In Figure 1, the converter is composed of an 18-pulse isolation transformer, 3 diode rectifier bridges, and the hybrid harmonic injection circuits; each injection circuit consist of an injection transformer, 3 diodes, a switch, and its control circuit.

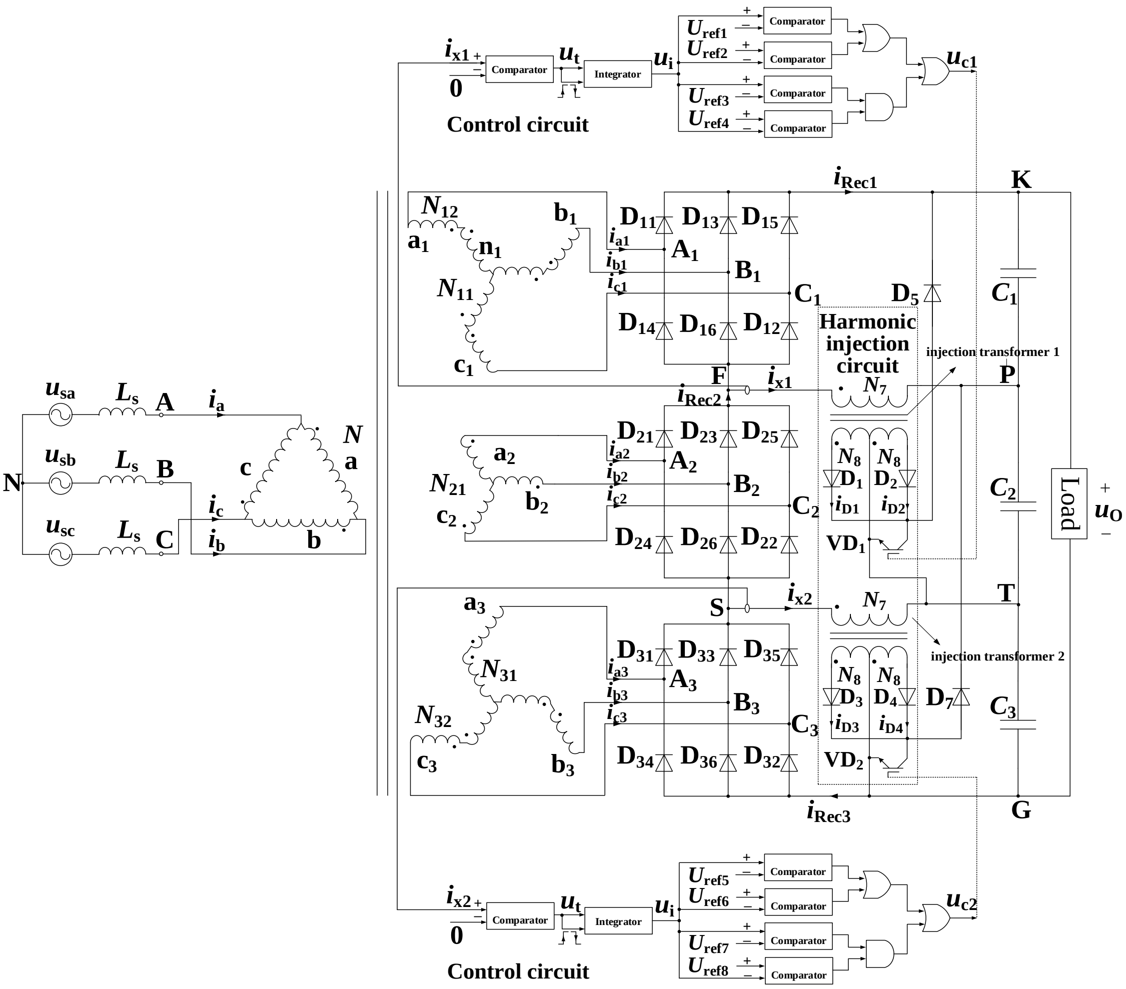

Figure 1. The proposed multipulse rectifier using hybrid harmonic reduction method.

According to the structure of the three-phase diode-bridge rectifier, the output voltage of each bridge has six pulse per supply cycle, and each pulse lasts 60°. In Figure 1, three-diode bridge rectifiers are connected in series. To suppress the harmonics of input current and ripples of load voltage to the highest degree, the phase difference of the input three-phase voltages of the diode bridge rectifiers is 20°, and Figure 2 describes the vector diagram.

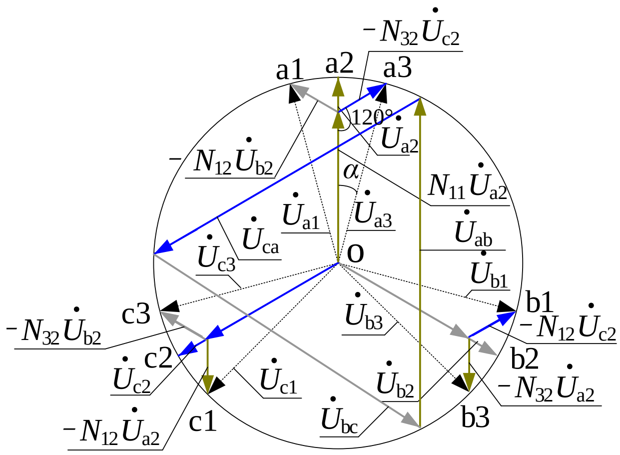

Figure 2. Vector diagram of the isolation transformer. a1, a2, a3, b1, b2, b3, c1, c2, c3 are the vectors of the output phases of the main transformer.

Take phase A as an example; from Figure 2, it can be obtained that

$$\begin{cases} \cos\alpha = \dfrac{(N_{11}U_{a2})^2 + {U_{a3}}^2 - (N_{32}U_{c2})^2}{2N_{11}U_{a2}U_{a3}} \\ \cos 120^\circ = \dfrac{(N_{11}U_{a2})^2 + (N_{32}U_{c2})^2 - {U_{a3}}^2}{2N_{11}U_{a2}N_{32}U_{c2}} \end{cases} \tag{1}$$

where N_{11} and N_{32} are the turn ratio of the phase-shifting transformer; U_{a2}, U_{a3}, and U_{c2} are the amplitude of the input voltages of the three-phase bridge.

From Equation (1), and Figures 1 and 2, when α is 20 degrees, the turn ratio of the isolation transformer meets the following:

$$N : N_{11} : N_{12} : N_{21} : N_{31} : N_{32} = \sqrt{3} : 0.742 : 0.395 : 1 : 0.742 : 0.395 \tag{2}$$

When the converter operates normally, the input voltage of the converter is described as

$$\begin{cases} u_{AN} = U\angle 0^\circ \\ u_{BN} = U\angle 120^\circ \\ u_{CN} = U\angle -120^\circ \end{cases} \tag{3}$$

where U is the amplitude of the input voltage.

From Figure 2 and Expression (3), the three sets of output voltages of the isolation transformer can be calculated as

$$\begin{cases} u_{a1} = \frac{U}{\sqrt{3}}\angle 10^\circ \\ u_{b1} = \frac{U}{\sqrt{3}}\angle 130^\circ \\ u_{c1} = \frac{U}{\sqrt{3}}\angle -110^\circ \end{cases} \begin{cases} u_{a2} = \frac{U}{\sqrt{3}}\angle 30^\circ \\ u_{b2} = \frac{U}{\sqrt{3}}\angle 150^\circ \\ u_{c2} = \frac{U}{\sqrt{3}}\angle -90^\circ \end{cases} \begin{cases} u_{a3} = \frac{U}{\sqrt{3}}\angle 50^\circ \\ u_{b3} = \frac{U}{\sqrt{3}}\angle 170^\circ \\ u_{c3} = \frac{U}{\sqrt{3}}\angle -70^\circ \end{cases} \tag{4}$$

2.2. Operating Modes Analyse

In Figure 1, according to the KCL, the currents through the primary winding of the injection transformers are described as

$$\begin{cases} i_{x1} = i_{Rec2} - i_{Rec1} \\ i_{x2} = i_{Rec3} - i_{Rec2} \end{cases} \tag{5}$$

where i_{x1} and i_{x2} are the currents through the primary windings of injection transformers 1 and 2, respectively.

Under constant-voltage load, based on the topology of the three-phase diode bridge rectifier, Figure 3 describes the output currents (i_{Rec1}, i_{Rec2}, i_{Rec3}) of the rectifier bridges; and from Equation (4), the currents i_{x1} and i_{x2} can also be obtained, as shown in Figure 3.

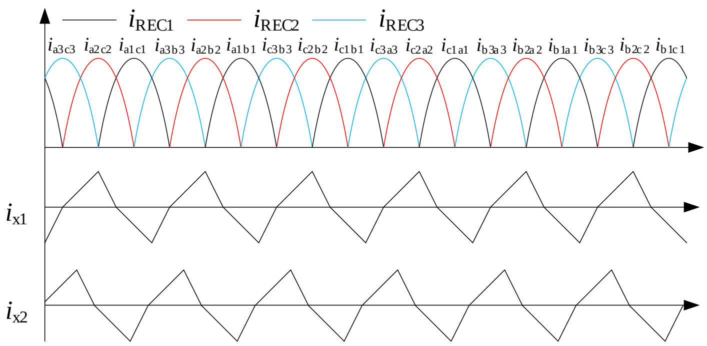

Figure 3. Operating waveforms of the converter.

According to Figure 1, when the input voltage of the converter is harmonic-free, and Equation (4) is calculated as follows.

$$\begin{cases} u_{a1} = \frac{U_{AN}}{\sqrt{3}}\angle 10^\circ = \frac{U}{\sqrt{3}}\sin(\omega t + 10^\circ) \\ u_{b1} = \frac{U_{BN}}{\sqrt{3}}\angle 10^\circ = \frac{U}{\sqrt{3}}\sin(\omega t + 130^\circ) \\ u_{c1} = \frac{U_{CN}}{\sqrt{3}}\angle 10^\circ = \frac{U}{\sqrt{3}}\sin(\omega t - 110^\circ) \end{cases} \begin{cases} u_{a2} = \frac{U_{AN}}{\sqrt{3}}\angle 30^\circ = \frac{U}{\sqrt{3}}\sin(\omega t + 30^\circ) \\ u_{b2} = \frac{U_{BN}}{\sqrt{3}}\angle 30^\circ = \frac{U}{\sqrt{3}}\sin(\omega t + 150^\circ) \\ u_{c2} = \frac{U_{CN}}{\sqrt{3}}\angle 30^\circ = \frac{U}{\sqrt{3}}\sin(\omega t - 90^\circ) \end{cases} \begin{cases} u_{a3} = \frac{U_{AN}}{\sqrt{3}}\angle 50^\circ = \frac{U}{\sqrt{3}}\sin(\omega t + 50^\circ) \\ u_{b3} = \frac{U_{BN}}{\sqrt{3}}\angle 50^\circ = \frac{U}{\sqrt{3}}\sin(\omega t + 170^\circ) \\ u_{c3} = \frac{U_{CN}}{\sqrt{3}}\angle 50^\circ \approx \frac{U}{\sqrt{3}}\sin(\omega t - 70^\circ) \end{cases} \tag{6}$$

From Equation (6), the output voltages of the rectifier bridges are described as Figure 4. In Figure 4, the voltages u_{KF}, u_{FS}, and u_{SG} have 6 pulses per supply cycle with a phase difference of 20 degrees, and each pulse lasts 60 degrees.

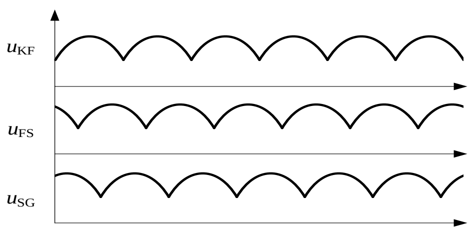

Figure 4. Output voltages of the rectifier bridges.

From Figure 1, the injection voltages u_{FP} and u_{ST} are calculated as

$$\begin{cases} u_{FP} = \frac{u_{FS} + u_{SG} - u_{KF}}{2} - \frac{u_o}{6} \\ u_{ST} = \frac{u_{SG} - u_{KF} - u_{FS}}{2} + \frac{u_o}{6} \end{cases} \tag{7}$$

where u_{FP} and u_{ST} are the primary winding voltages of the two injection transformers, respectively.

From Figure 4 and Equation (6), the injection voltages u_{FP} and u_{ST} can be described as in Figure 5.

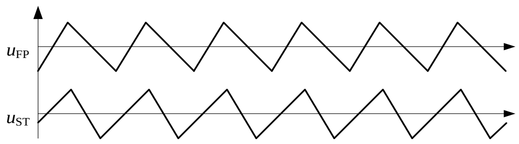

Figure 5. Primary winding voltages of the injection transformers when input voltage of the rectifier is harmonic-free.

From [12–14], almost all the harmonic reduction methods generate multistep waveforms which are equivalent to the ideal injection waveform (as shown in Figure 5) to suppress harmonics. That is because the cost and difficulty of generating multistep waves are much lower than these of the triangular waves. Besides, the harmonic reduction effects of the multistep wave and the triangular wave are similar.

From Figure 5, there are three combinations of currents i_{x1} and i_{x2}, which are ① $i_{x1} > 0$, $i_{x2} > 0$, ② $i_{x1} > 0$, $i_{x2} < 0$, ③ $i_{x1} < 0$, $i_{x2} > 0$. On the basis of the on–off state of VD_1, VD_2, and the currents i_{x1} and i_{x2}, the harmonic suppression circuit has seven modes, described as Figure 6.

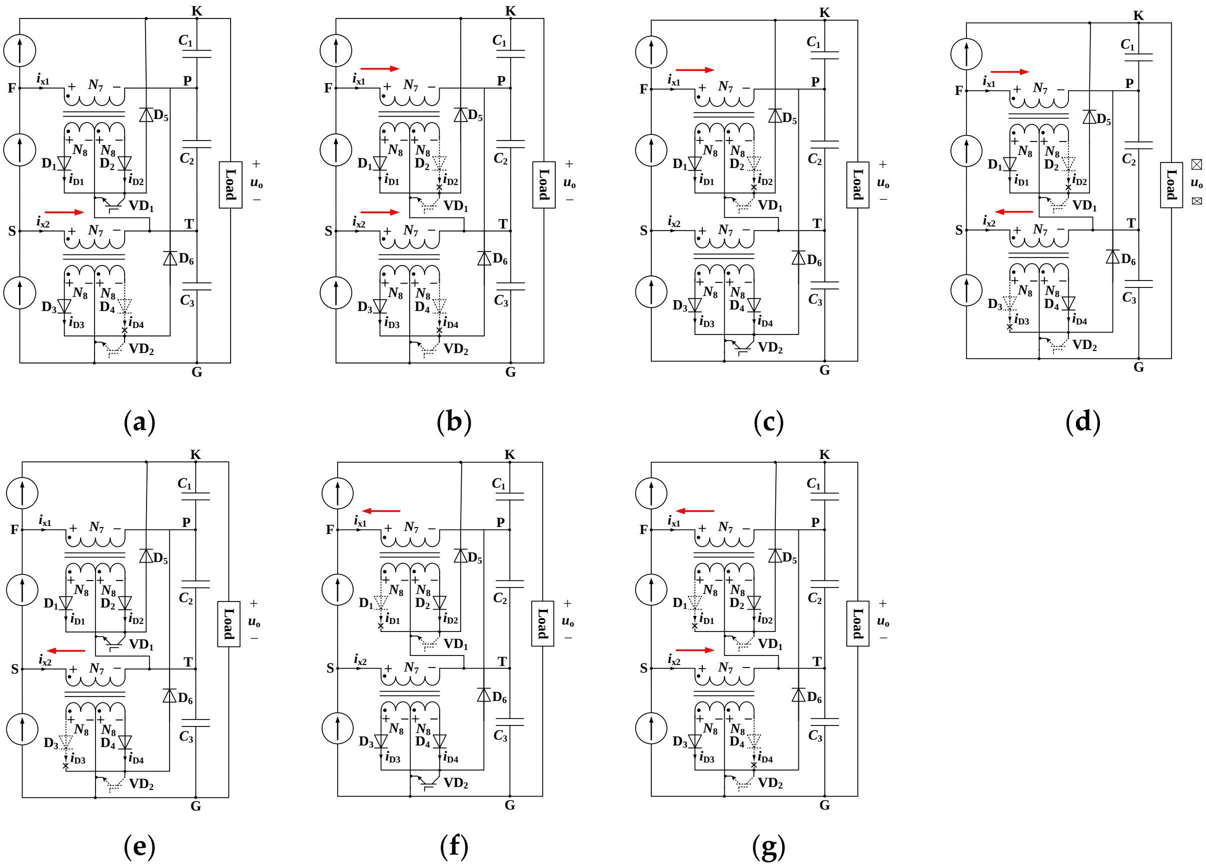

Figure 6. Operating modes of the harmonic injection circuit. (**a**) Mode. 1. (**b**) Mode. 2. (**c**) Mode. 3. (**d**) Mode. 4. (**e**) Mode. 5. (**f**) Mode. 6. (**g**) Mode. 7. The red arrows represents the directions of currents i_{x1} and i_{x2}.

In Figure 6a, VD_1 is turned on, VD_2 is turned off, $i_{x2} > 0$, D_1, D_2 and D_3 are forward-biased, D_4 is revise-biased, and the injection voltages u_{FP} and u_{ST} are calculated as

$$\begin{cases} u_{FP} = 0 \\ u_{ST} = \dfrac{2N_7}{3N_8} u_o \end{cases} \tag{8}$$

In Figure 6b, VD_1 and VD_2 are turned off, $i_{x1} > 0$, $i_{x2} > 0$, D_1 and D_3 are forward-biased, D_2 and D_4 are revise-biased, and the injection voltages u_{FP} and u_{ST} are calculated as

$$\begin{cases} u_{FP} = \dfrac{2N_7}{3N_8} u_o \\ u_{ST} = \dfrac{2N_7}{3N_8} u_o \end{cases} \tag{9}$$

In Figure 6c, VD_1 is turned off, VD_2 is turned on, $i_{x1} > 0$, D_1, D_3 and D_4 are forward-biased, D_2 is revise-biased, and the injection voltages u_{FP} and u_{ST} are calculated as

$$\begin{cases} u_{FP} = \dfrac{2N_7}{3N_8} u_o \\ u_{ST} = 0 \end{cases} \tag{10}$$

In Figure 6d, VD_1 and VD_2 are turned off, D_1 and D_4 are forward-biased, D_2 and D_3 are revise-biased, and the injection voltages u_{FP} and u_{ST} are calculated as

$$\begin{cases} u_{FP} = \dfrac{2N_7}{3N_8} u_o \\ u_{ST} = -\dfrac{2N_7}{3N_8} u_o \end{cases} \tag{11}$$

In Figure 6e, VD_1 is turned on, VD_2 is turned off, D_1, D_2 and D_4 are forward-biased, D_3 is revise-biased, and the injection voltages u_{FP} and u_{ST} are calculated as

$$\begin{cases} u_{FP} = 0 \\ u_{ST} = -\dfrac{2N_7}{3N_8} u_o \end{cases} \tag{12}$$

In Figure 6f, VD_1 is turned off, VD_2 is turned on, D_2, D_3 and D_4 are forward-biased, D_1 is revise-biased, and the injection voltages u_{FP} and u_{ST} are calculated as

$$\begin{cases} u_{FP} = -\dfrac{2N_7}{3N_8} u_o \\ u_{ST} = 0 \end{cases} \tag{13}$$

In Figure 6g, VD_1 and VD_2 are turned off, D_2 and D_3 are forward-biased, D_1 and D_4 are revise-biased, and the injection voltages u_{FP} and u_{ST} are calculated as

$$\begin{cases} u_{FP} = -\dfrac{2N_7}{3N_8} u_o \\ u_{ST} = \dfrac{2N_7}{3N_8} u_o \end{cases} \tag{14}$$

From Equations (7)–(13), and Figures 5 and 6, the injection voltage of the converter can be obtained, as shown in Figure 7. In Figure 7, there are 48 combinations per power supply cycle; and in order to suppress the $(18k \pm 1)$th and $(36k \pm 1)$th harmonics, the duration of combinations 6, 14, 22, 30, 38, and 46 is 1/27 power supply cycle, and the duration of the other combinations is 1/54 power supply cycle.

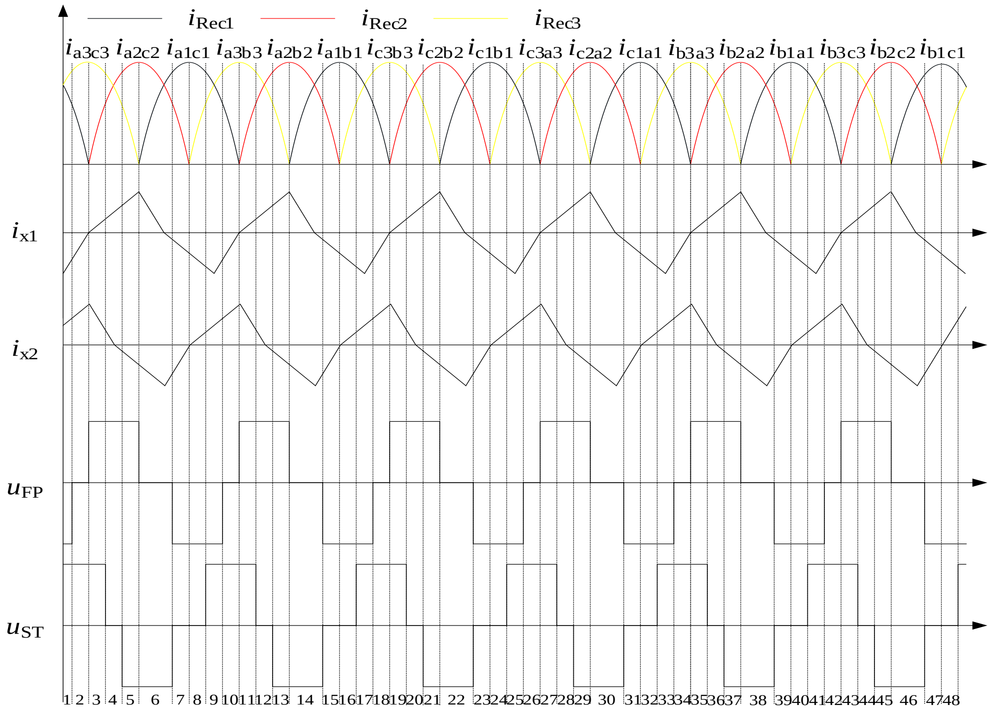

Figure 7. Operating waveforms of the proposed rectifier.

3. Injection Transformer Turned Ratio Calculation

The following analysis takes combination 5 as an example. In combination 5, $i_{a2} > 0$, $i_{b2} = 0$, $i_{c2} < 0$, $i_{a3} > 0$, $i_{b3} = 0$, $i_{c3} < 0$. Therefore, voltage u_{a2c2} and voltage u_{a3c3} are calculated as

$$\begin{cases} u_{a2c2} = \dfrac{(N_8 + 4N_7)}{3N_8} u_o \\ u_{a3c3} = \dfrac{(N_8 - 2N_7)}{3N_8} u_o \end{cases} \tag{15}$$

From Figures 2 and 3, it is obtained that

$$u_{a1c1} = N_2 u_{n2b2} + N_1 u_{a2n2} + N_1 u_{n2c2} + N_2 u_{a2n2} \tag{16}$$

where $N_1 = N_{11}/N_{21} = N_{31}/N_{21}$, $N_2 = N_{12}/N_{21} = N_{32}/N_{21}$.

From above analysis, u_{b2c2} can be expressed as

$$u_{b2c2} = \frac{(N_8 - N_7 - N_1 N_8 - 4N_1 N_7)}{3N_2 N_8} u_o \tag{17}$$

Then, u_{a2b2} is expressed as

$$u_{a2b2} = \frac{(N_2 N_8 - 2N_2 N_7 - N_8 - 2N_7 + N_1 N_8 - 2N_1 N_7)}{3N_2 N_8} u_o \tag{18}$$

According to Equation (18) and the structure of the isolation transformer, voltage u_{AN} can be obtained as follows:

$$u_{AN} = \frac{5(N_2 N_8 - 2N_2 N_7 - N_8 - 2N_7 + N_1 N_8 - 2N_1 N_7)}{3\sqrt{3} N_2 N_8} u_o \tag{19}$$

Similarly, the expressions of voltage u_{AN} in one supply cycle can also be obtained, as shown in Table 1.

Table 1. Expressions of Voltage u_{AN} with the harmonic suppression method.

Voltage	Level	Voltage	Level
u_1	$\frac{5(N_8+4N_7)}{3\sqrt{3}N_8}u_o$	u_7	$\frac{5(N_8+2N_7-N_1N_8+2N_1N_7)}{3\sqrt{3}N_2N_8}u_o$
u_2	$\frac{5(N_8+2N_7)}{3\sqrt{3}N_8}u_o$	u_8	$\frac{5(N_8-N_1N_8-2N_1N_7)}{3\sqrt{3}N_2N_8}u_o$
u_3	$\frac{5(N_8-2N_7)}{3\sqrt{3}N_8}u_o$	u_9	$\frac{5(N_8-N_7-N_1N_8-4N_1N_7)}{3\sqrt{3}N_2N_8}u_o$
u_4	$\frac{5(N_1N_8+2N_1N_7-N_2N_8)}{3\sqrt{3}N_8(N_1^2-N_2^2)}u_o$	u_{10}	$\frac{5(N_2N_8+2N_2N_7-N_8+N_1N_8+2N_1N_7)}{3\sqrt{3}N_2N_8}u_o$
u_5	$\frac{5(N_1N_8+2N_1N_7-N_2N_8-2N_2N_7)}{3\sqrt{3}N_8(N_1^2-N_2^2)}u_o$	u_{11}	$\frac{5(N_2N_8-2N_2N_7-N_8-2N_7+N_1N_8-2N_1N_7)}{3\sqrt{3}N_2N_8}u_o$
u_6	$\frac{5(N_1^2N_8-N_1N_2N_8-2N_1N_2N_7)}{3\sqrt{3}N_1N_8(N_1^2-N_2^2)}u_o$	u_{12}	$\frac{10N_7}{3\sqrt{3}N_8(N_1-N_2)}u_o$

Based on Table 1, the waveform of u_{AN} in one supply cycle can be obtained, as shown in Figure 8.

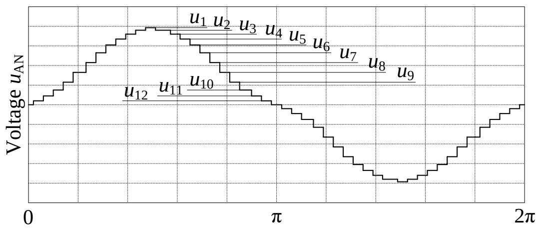

Figure 8. Voltage u_{AN} in one supply cycle.

According to Figure 8 and Table 1, the RMS value and the fundamental value of the input voltage can be calculated as Equations (20) and (21), respectively.

$$U_{S1} = \frac{1}{0.2806N_8\pi}\left\{\begin{array}{l} -4.266N_8 + 0.373N_8\cos\frac{\pi}{18} + 0.167N_8\cos\frac{7\pi}{54} + 0.132N_8\sin\frac{\pi}{9} \\ +6.875N_7 - 2.776N_7\cos\frac{\pi}{18} - 8.549N_7\cos\frac{5\pi}{54} - 1.213\cos\frac{7\pi}{54} - 0.54\cos\frac{\pi}{27} - 2.162\sin\frac{2\pi}{27} \\ +1.081\sin\frac{\pi}{9} + 6.222N_7\cos\frac{\pi}{54} - 0.156\cos\frac{11\pi}{54} - 0.624\cos\frac{13\pi}{54} + 0.624\sin\frac{4\pi}{27} \\ -0.653N_8 - 1.508N_7 + 11.793N_7\cos\frac{7\pi}{54} + 1.508N_7\sin\frac{\pi}{27} + 6.031N_7\sin\frac{2\pi}{27} - 7.706N_7\sin\frac{\pi}{9} \\ -3.479N_7\cos\frac{11\pi}{54} - 13.916N_7\cos\frac{13\pi}{54} + 5.05N_7\sin\frac{2\pi}{9} - 3.817N_8\sin\frac{2\pi}{9} + 4.06N_7\sin\frac{5\pi}{27} \end{array}\right\} \tag{20}$$

$$U_{AN} == \frac{1}{3\sqrt{3}}\sqrt{\frac{7.337N_8^2 + 123.655N_7^2 + 16.377N_7N_8}{N_8^2}} \tag{21}$$

According to Equations (20) and (21), the relation between the input voltage THD and the injection transformer turn ratio can is described in Figure 9.

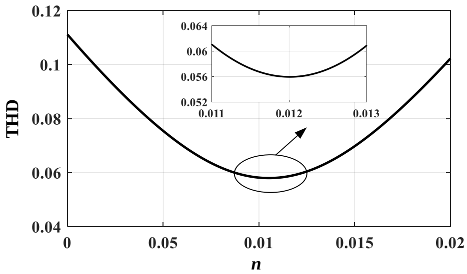

Figure 9. The relationship between the THD of input voltage and the turn ratio of injection transformers.

From Figure 9, when the turns ratio (n) is 0.0118, the THD of input voltage reaches the minimum value 0.0588.

From Table 1 and Figure 9, the expressions of input voltages harmonics with harmonic suppression circuit can be obtained, written as follows:

$$u_{\text{Har}-48} = \sum_{n=6k\pm1}^{\infty} \frac{1}{0.2806 N_8 \pi} \left\{ \begin{array}{l} -4.266N_8 + 0.373N_8 \cos\frac{n\pi}{18} + 0.167N_8 \cos\frac{7n\pi}{54} + 0.132N_8 \sin\frac{n\pi}{9} \\ +6.875N_7 - 2.776N_7 \cos\frac{n\pi}{18} - 8.549N_7 \cos\frac{5n\pi}{54} - 1.213 \cos\frac{7n\pi}{54} \\ -0.54 \cos\frac{n\pi}{27} - 2.162 \sin\frac{2n\pi}{27} + 1.081 \sin\frac{n\pi}{9} + 6.222N_7 \cos\frac{n\pi}{54} \\ -0.156 \cos\frac{11n\pi}{54} - 0.624 \cos\frac{13n\pi}{54} + 0.624 \sin\frac{4n\pi}{27} - 0.653N_8 \\ -1.508N_7 + 11.793N_7 \cos\frac{7n\pi}{54} + 1.508N_7 \sin\frac{n\pi}{27} + 6.031N_7 \sin\frac{2n\pi}{27} \\ -7.706N_7 \sin\frac{n\pi}{9} - 3.479N_7 \cos\frac{11n\pi}{54} - 13.916N_7 \cos\frac{13n\pi}{54} \\ +5.05N_7 \sin\frac{2n\pi}{9} - 3.817N_8 \sin\frac{2n\pi}{9} + 4.06N_7 \sin\frac{5n\pi}{27} \end{array} \right\} \sin nx \quad (22)$$

From Equation (22), after using the proposed suppression method, the $(18k \pm 1)$th and $(36k \pm 1)$th harmonics of the input voltages are reduced.

4. Capacity of the Proposed Harmonic Reduction Circuit

To estimate the harmonic suppression cost of the proposed hybrid method, the capacity of the injection transformer and the loss of the switches are analyzed. From Figure 7, the injection voltage u_{FP} and u_{ST} are calculated as

$$u_{\text{FP}} = \begin{cases} 0 \; [\frac{k\pi}{3}, \frac{\pi}{27} + \frac{k\pi}{3}] \cup \left[\frac{4\pi}{27} + \frac{k\pi}{3}, \frac{2\pi}{9} + \frac{k\pi}{3}\right] \\ 0.0079u_o \; [\frac{\pi}{27} + \frac{k\pi}{3}, \frac{4\pi}{27} + \frac{k\pi}{3}] \\ -0.0079u_o \; [\frac{2\pi}{9} + \frac{k\pi}{3}, \frac{(k+1)\pi}{3}] \end{cases} \quad u_{\text{ST}} = \begin{cases} 0 \; [\frac{\pi}{9} + \frac{k\pi}{3}, \frac{5\pi}{27} + \frac{k\pi}{3}] \cup \left[\frac{8\pi}{27} + \frac{k\pi}{3}, \frac{(k+1)\pi}{3}\right] \\ 0.0079u_o \; [\frac{5\pi}{27} + \frac{k\pi}{3}, \frac{8\pi}{27} + \frac{k\pi}{3}] \\ -0.0079u_o \; [\frac{(k+1)\pi}{3}, \frac{\pi}{9} + \frac{(k+1)\pi}{3}] \end{cases} \quad (23)$$

From Figures 1 and 7, the injection current i_{x1} and i_{x2} are calculated as

$$\begin{aligned} i_{\text{x1}} &= 3 \begin{cases} \frac{9I_o}{\pi}x - \frac{I_o}{3} \; [\frac{\pi}{27} + \frac{k\pi}{3}, \frac{4\pi}{27} + \frac{k\pi}{3}] \\ -\frac{54I_o}{7\pi}x + \frac{11I_o}{7} \; [\frac{4\pi}{27} + \frac{k\pi}{3}, \frac{11\pi}{54} + \frac{k\pi}{3}] \\ -\frac{9I_o}{\pi}x + \frac{11I_o}{6} \; [\frac{11\pi}{54} + \frac{k\pi}{3}, \frac{17\pi}{54} + \frac{k\pi}{3}] \\ \frac{6I_o}{\pi}x - \frac{20I_o}{9} \; [\frac{17\pi}{54} + \frac{k\pi}{3}, \frac{10\pi}{27} + \frac{k\pi}{3}] \end{cases} \\ i_{\text{x2}} &= i_{\text{x1}} \angle 30^\circ \end{aligned} \quad (24)$$

From Equations (23) and (24), Equation (25) describes the injection transformer capacity.

$$S = u_{\text{FP}} i_{\text{x1}} + u_{\text{ST}} i_{\text{x2}} \approx 0.019 u_o i_o \quad (25)$$

From Equation (25), the injection transformer capacity is only 1.9% of the output power. As discussed in [11–16], the injection transformers capacity of the existing methods was higher than 2% of load power. Therefore, the circuit loss of the proposed suppression method is reduced to a certain extent.

According to Figure 9, the current across the secondary side of the injection transformer is 0.0118 times of the primary side. Assuming the load power is 1500 W and the drain source on-state resistance of the switch is 500 mΩ, the loss of the switch is calculated as 5 × 0.0118 × 0.5 = 0.0295 W. Therefore, the switch loss of the switch can be approximately neglected.

5. Simulation and Experiment Validation

To verify the above analysis, some experiments were carried out. The parameters of the rectifier are described as follows.

1. The turns ratio of the main transformer meets that N:N_{11}:N_{12}:N_{21}:N_{31}:N_{32} = $5\sqrt{3}$:0.742:0.395:1:0.742:0.395.
2. The injection transformer turns ratio meets that N_7:N_8 = 0.0118.
3. The RMS of the power supply is 220 V, and the frequency is 50 Hz.

Figure 10 describes the prototype of the proposed multipulse rectifier. In Figure 10, the control circuit is a combination of the sampling circuit, the drive circuit, and the rapid control typing (RCP).

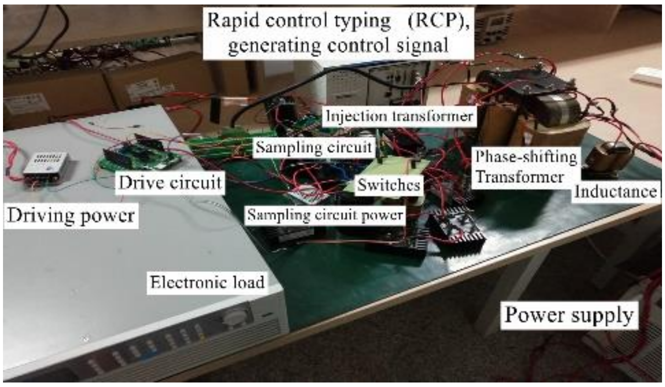

Figure 10. The prototype of the proposed rectifier.

When without the suppression method, the input voltage of the rectifier is described as Figure 11. The input voltage in Figure 11 has 18 steps per cycle, the simulated THD of input voltage is 8.7%. Because of the leakage inductance of the main transformer, the experimental value is about 6.8%.

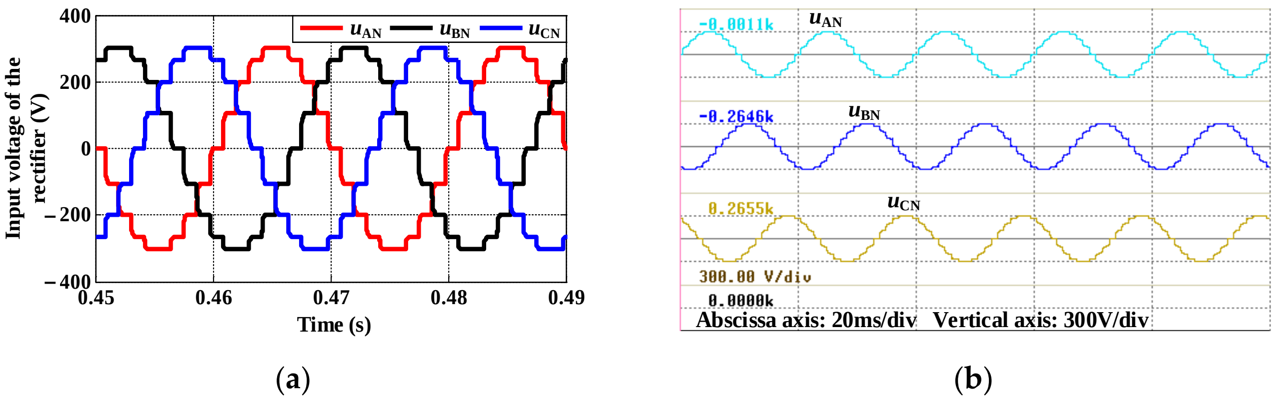

Figure 11. Input voltage of the 18-pulse rectifier without the reduction method. (**a**) Simulation result. (**b**) Experimental result.

When using the suppression method, Figure 12 shows the input voltages of the rectifier. In Figure 12, the input voltages are sinusoids, the simulated THD of input voltage is 3.6%. Similarly, because of the leakage inductance of the main transformer, the experimental THD of input voltage is about 2.4%.

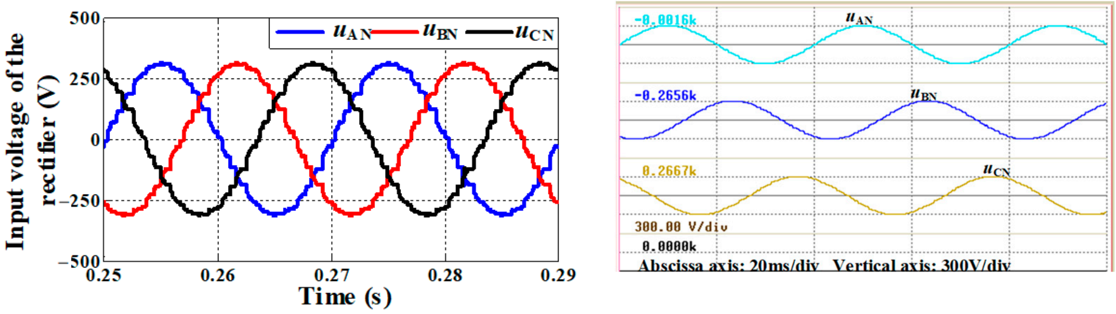

(**a**) (**b**)

Figure 12. Input voltage of the proposed rectifier with the reduction method. (**a**) Simulation result. (**b**) Experimental result.

Figure 13 expresses the input currents when without suppression method. In Figure 13, the simulated THD is about 7.4%, and the experimental THD is about 5.8%.

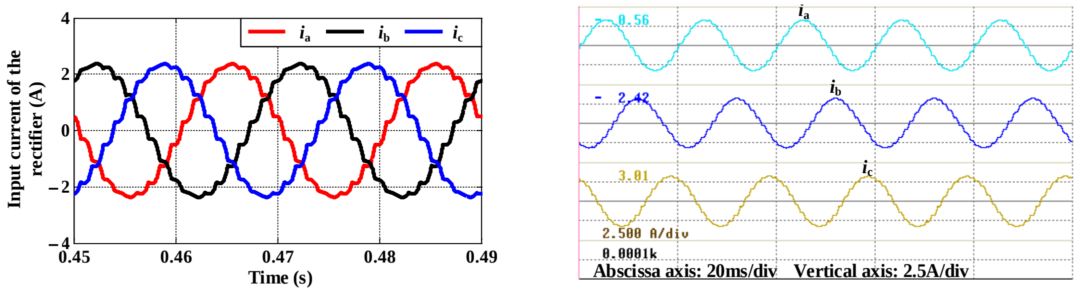

(**a**) (**b**)

Figure 13. Input current of the rectifier without the reduction method. (**a**) Simulation result. (**b**) Experimental result.

Figure 14 shows the input currents when using the hybrid harmonic reduction method. In Figure 14, the simulated THD is about 3.1%, and the experimental value is about 2.7%.

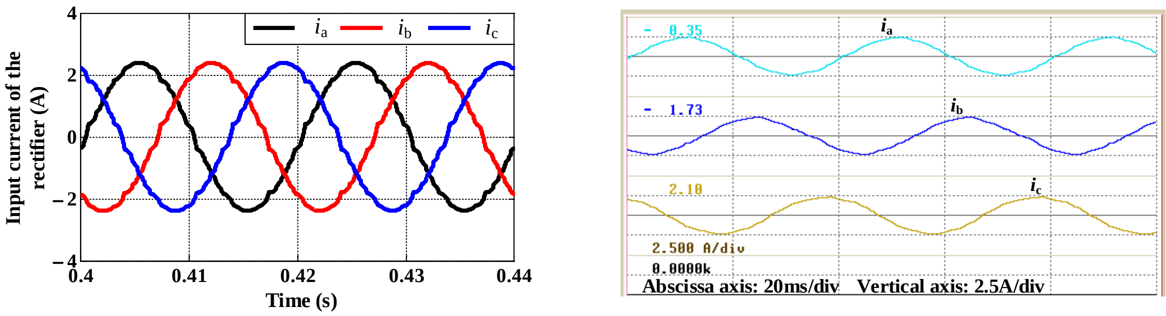

(**a**) (**b**)

Figure 14. Input current of the converter with the reduction method. (**a**) Simulation result. (**b**) Experimental result.

From Figures 11–14, after using the harmonic suppression method, the simulated THD of input voltage decreases from 8.7 to 3.6%, and the experimental THD decreases from 6.8 to 2.4%; the simulated THD of input current decreases from 7.4 to 3.1%, and the experimental THD decreases from 5.8 to 2.7%. Therefore, the hybrid harmonic reduction method can suppress harmonics of the input side.

Figure 15 shows the output voltage current of the proposed rectifier. In Figure 15, the voltage and current remain approximately constant, and the load voltage and load current are around 310 V and 3.4 A, respectively; the output power is calculated as 1100 W. From Figure 15a,b, it can be obtained that the simulation and experiment results are basically the same.

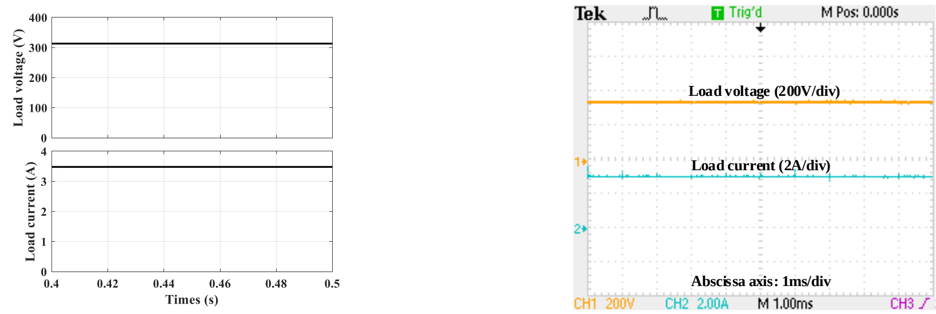

(**a**) (**b**)

Figure 15. Output voltage and output current of the proposed rectifier. (**a**) Simulation result. (**b**) Experimental result.

Figures 16 and 17 show the current through and voltage across the primary winding of the injection transformer, respectively. In Figure 16, the current is triangular wave with a frequency of 300 Hz. In Figure 17 the is three-step waveform with a frequency of 300 Hz.

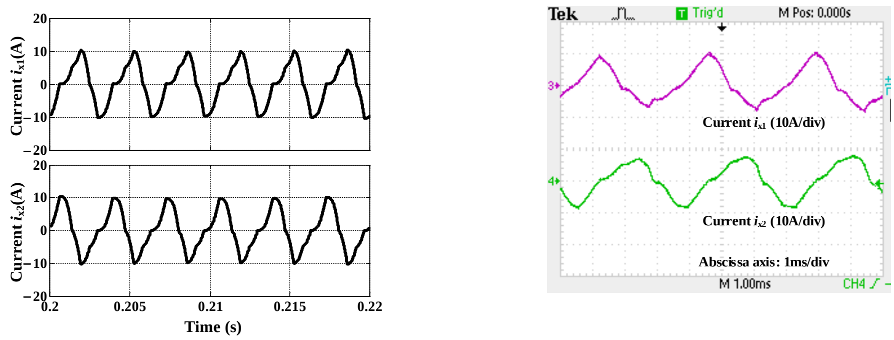

(**a**) (**b**)

Figure 16. Current through the primary winding of the injection transformer. (**a**) Simulation result. (**b**) Experimental result.

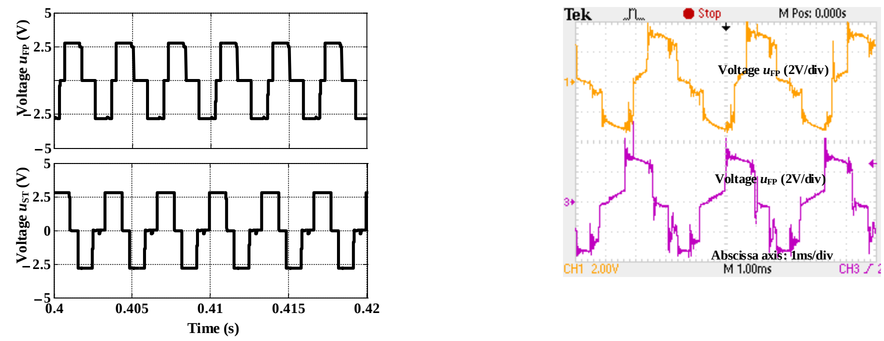

(**a**) (**b**)

Figure 17. Voltage across the primary winding of the injection transformer. (**a**) Simulation result. (**b**) Experimental result.

From Figures 16 and 17, the amplitude of the current is around 8.5 A, the amplitude of the voltage is 2.4 V. Therefore, the capacity of each injection transformer is about 10 W, which is about 1% of the load power. Because of the leakage inductance of the main transformer, the experimental results of current i_{x1} and current i_{x2} in Figure 16b have some distortion. Because of the mode switch of VD_1 and VD_2, the experimental results of the injection voltages in Figure 17b have some spikes in the switching instant.

Figure 18a describes the load voltage and load current of the proposed rectifier when the load resistance changes from 180 to 90 Ω. Figure 18b shows the input current of A phase when the load changes from 180 to 90 Ω. From Figure 18a it can be obtained that the output voltage remains constant while the output current has a step change. From Figure 18b, it can be acquired that the input current rises gently when the load is switching, but the THD value of the input does not change.

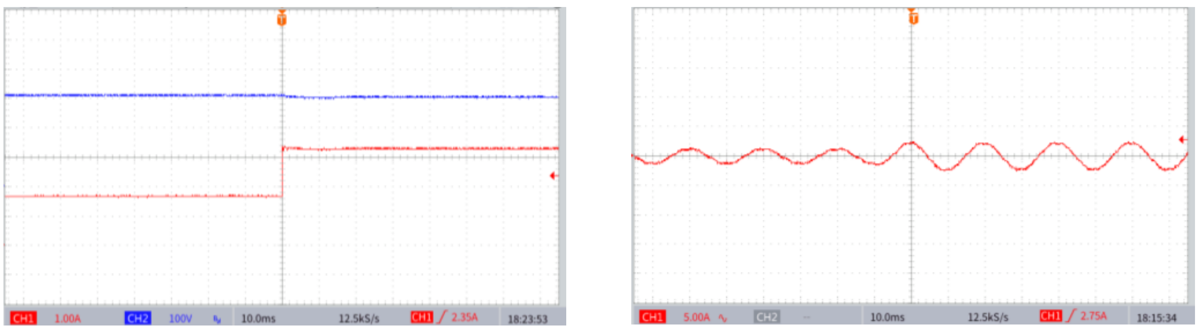

(**a**) (**b**)

Figure 18. The input and output of the rectifier when the load changes. (**a**) Simulation result. (**b**) Experimental result.

6. Conclusions

To suppress the harmonics of input voltage, this paper proposed a multipulse rectifier which combines multiple output transformer (nine outputs and above) and the hybrid harmonic suppression method. The proposed rectifier not only can improve the output voltage level, but also improve the input power quality. Through injecting two sets of six-times three-step voltages with a phase difference of 20 degree at DC link, the $(18k \pm 1)$th and $(36k \pm 1)$th harmonics of input voltages are significantly suppressed. When using harmonic reduction method, the experimental THD of the input voltages is reduced from 6.8 to 2.4%, and the experimental THD of the input currents is reduced from 5.8 to 2.7%, and the output voltage and output current remain constant. Under some experimental conditions, the capacity of the hybrid harmonic reduction is only about 1% of load power. The proposed converter is qualified for the interface between the AC generator and the DC bus of the aircraft electrical system.

Author Contributions: Conceptualization, Q.L.; methodology, Q.L. and X.Y.; software, F.M.; formal analysis, Q.L.; investigation, X.H.; data curation, G.W.; writing—original draft preparation, C.G.; writing—review and editing, Q.L.; visualization, Q.L. and X.Y.; supervision, F.M.; project administration, X.H.; funding acquisition, F.M. All authors have read and agreed to the published version of the manuscript.

Funding: National Natural Science Foundation of China, 51777042.

Institutional Review Board Statement: Not applicable.

Informed Consent Statement: Not applicable.

Data Availability Statement: Data available on request from the authors.

Conflicts of Interest: The authors declare no conflict of interest.

References

1. Meng, F.G.; Yang, S.Y.; Yang, W. Summary of Multi-pulse Rectifier. *Electron. Power Autom. Equip.* **2012**, *32*, 9–22.
2. Du, Q.; Gao, L.; Li, Q.; Liu, W.; Yin, X.; Meng, F. Harmonic Reduction Methods at DC Link of Series-Connected Multi-Pulse Rectifiers: A Review. *IEEE Trans. Power Electron.* **2022**, *37*, 3143–3160. [CrossRef]
3. Zhang, P.; Chen, Q.; Mao, L. A type 18-pulse isolation transformer. *J. Nanjing Univ. Aeronaut. Astronaut.* **2014**, *46*, 129–136.
4. Young, C.M.; Wu, S.F.; Yeh, W.S.; Yeh, C.W. A DC-Side Current Injection Method for Improving AC Line Condition Applied in the 18-Pulse Converter System. *IEEE Trans. Power Electron.* **2014**, *29*, 99–109. [CrossRef]
5. Nguyen, T.H.; Lee, D.C.; Kim, C.K. A Series-Connected Topology of a Diode Rectifier and a Voltage-Source Converter for an HVDC Transmission System. *IEEE Trans. Power Electron.* **2014**, *29*, 1579–1584. [CrossRef]
6. Yuan, D.S.; Wang, S.H.; Zhang, H.J.; Tao, X.; Zhu, J.G.; Guo, Y.G. The Harmonic Suppression Characteristic Analysis of a Phase-Shifting Reactor in Rectifier System. *IEEE Trans. Magn.* **2015**, *51*, 1–4. [CrossRef]
7. Singh, B.; Bhuvaneswari, G.; Garg, V. An Improved Power-Quality 30-Pulse AC–DC for Varying Loads. *IEEE Trans. Power Deliv.* **2007**, *22*, 1179–1187. [CrossRef]
8. Guimaraes, C.; Olivier, G.; April, G.E. High Current AC/DC Power Converters using T-connected Transformers. In Proceedings of the 1995 Canadian Conference on Electrical and Computer Engineering, Montreal, QC, Canada, 5–8 September 1995.
9. Daniel, M.Z.; Paul, I.N.; Tao, J.; Joseph, S.M. An Improved Topology for Multipulse AC/DC Converters Within HVDC and VFD Systems: Operation in Degraded Modes. *IEEE Trans. Ind. Electron.* **2018**, *65*, 3646–3656.
10. Lyubov, R.; Anton, G.; Anton, M. Installed Power of Transformers for Equivalent Multiphase Rectification Circuits. In Proceedings of the 2019 International Conference on Electrotechnical Complexes and Systems, Ufa, Russia, 21–25 October 2019.
11. Wang, T.J.; Fang, F.; Jiang, X.Y.; Wang, K.Y.; Yang, L. Performance and Design Analysis on Round-Shaped Transformers Applied in Rectifier Systems. *IEEE Trans. Ind. Electron.* **2017**, *64*, 948–955. [CrossRef]
12. Meng, F.G.; Qing, X.D.; Wang, L.; Gao, L.; Man, Z.C. A Series-Connected 24-Pulse Rectifier Using Passive Voltage Harmonic Injection Method at DC-Link. *IEEE Trans. Power Electron.* **2019**, *34*, 8503–8512. [CrossRef]
13. Liu, Y.H.; Arrillaga, J.; Watson, N.R. A new high-pulse voltage-sourced converter for HVDC transmission. *IEEE Trans. Power Deliv.* **2003**, *18*, 1388–1393. [CrossRef]
14. Bai, S.; Lukic, S.M. New Method to Achieve AC Harmonic Elimination and Energy Storage Integration for 12-Pulse Diode Rectifiers. *IEEE Trans. Ind. Electron.* **2013**, *60*, 2547–2554. [CrossRef]
15. Chivite-Zabalza, F.J.; Forsyth, A.J.; Araujo-Vargas, I. 36-pulse hybrid ripple injection for high-performance aerospace rectifiers. *IEEE Trans. Ind. Appl.* **2009**, *45*, 992–999. [CrossRef]
16. Li, Q.H.; Meng, F.G.; Gao, L.; Zhang, H.Q.; Du, Q.X. A 30-Pulse Rectifier Using Passive Voltage Harmonic Injection Method at DC Link. *IEEE Trans. Ind. Electron.* **2020**, *67*, 9273–9291. [CrossRef]